SCIENCE CHINA
Chemistry

• ARTICLES •

March 2017 Vol.60 No.3: 370–376
doi: 10.1007/s11426-016-0159-2

Synthesis of aptamer-functionalized Ag nanoclusters for MCF-7 breast cancer cells imaging

Taotao Li[1], Jingjing Yang[2], Zeeshan Ali[1], Zunliang Wang[1], Xianbo Mou[1], Nongyue He[1*] & Zhifei Wang[2*]

[1]*State Key Laboratory of Bioelectronics, School of Biological Science and Medical Engineering, Southeast University, Nanjing 210096, China*
[2]*School of Chemistry and Chemical Engineering, Southeast University, Nanjing 210096, China*

Received April 10, 2016; accepted May 20, 2016; published online November 24, 2016

Aptamer-functionalized silver nanoclusters (Ag NCs) have been attracting a lot of interest as label-free probes which have been successfully applied to both cell imaging and molecular detection. MUC1 aptamer is an ssDNA aptamer that specifically binds to MUC1 mucin which is a large transmembrane glycoprotein whose expression level increases at least 10-fold in primary and metastatic breast cancers. Using C4A4C3-linker-MUC1 as template, the Ag NCs were synthesized through one-pot process. The fluorescence intensity of Ag NCs was found to be closely related to the length and type (poly adenine or thymine) of the linker, the optimum linker being –AAAAA–. Using the C4A4C3-A5-MUC1 as the scaffold, the synthesized Ag NCs emitted fluorescence with high quantum yield (QY) of 66.5%. Based on the specific interaction between the MUC1 aptamer and MUC1 mucin, the C4A4C3-A5-MUC1-stabilized Ag NCs could recognize and differentiate the MCF-7 breast cancer cells from MDA-MB-231 breast cancer and A549 human lung cancer cells.

MCF-7 cells, cell typing, Ag NCs, aptamer, one-pot process

Citation: Li T, Yang J, Ali Z, Wang Z, Mou X, He N, Wang Z. Synthesis of aptamer-functionalized Ag nanoclusters for MCF-7 breast cancer cells imaging. *Sci China Chem*, 2017, 60: 370–376, doi: 10.1007/s11426-016-0159-2

1 Introduction

DNA-templated aptamer-functionalized silver nanoclusters (Ag NCs) are widely used to detect DNA [1], RNA [2], protein [3], and inorganic ion [4]. Owing to their good properties which include high fluorescence intensity, photo stability, water solubility, and label-free detection, they are further applied in cell imaging [5–7]. Evidence indicates that four DNA nitrogenous bases show different affinity to Ag^+ and the strongest interaction was found to be between cytosine and Ag^+ [8–10]. The cytosine-rich DNA has therefore been preferentially employed to synthesize fluorescent Ag NCs [11–13]. Although the detailed mechanism for fluorescence from the DNA-templated Ag NCs is unclear, it has been widely adopted that their fluorescence properties greatly depend on the sequence and length of the DNA [14–16]. The fluorescence of DNA-stabilized Ag NCs can be tuned by varying the length and sequence of DNA template. With extensive research on aptamers [17–20] recently, aptamer-functionalized Ag NCs have been applied in CCRF-CEM cells [21], HeLa cells [22], Ramos cells [5], and MCF-7 cancer cells [6] recognition. The adopted DNA templates generally consisted of aptamer, linker and C_n (where n is the number of cytosine). The quantum yield (QYs) of the synthesized Ag NCs in these studies were lower than 5% except that the C12-T5-AS1411-stabilized Ag NCs synthesized by Li *et al*. [6] had the QY of 40.1%, which was

*Corresponding authors (email: nyhe1958@163.com; zfwang@seu.edu.cn)

© Science China Press and Springer-Verlag Berlin Heidelberg 2016

not bright enough for subsequent cell imaging. In order to obtain the Ag NCs with high QY, it is of interest to replace the C12 with other better DNA template.

Breast cancer is heterogeneous tumor with well-defined molecular subtypes, reported to be the most common cancer among women in the world. The identification of exact tumor subtypes in advance will improve breast cancer treatment efficacy. Several specific biomarkers have been discovered for breast cancer typing, these include glycoprotein, protein, and DNA [23]. The main technique for identification and determination of these biomarkers is immunohistochemistry (IHC) [24]. On the other hand, combining synthetic macromolecules and biomolecular recognition units are promising in developing novel diagnostic and analysis techniques for detecting clinically important substances. For example, the aptamers, which are single stranded DNA or RNA analogues to antibodies [25,26], have been attracting a lot of interest due to their advantages over traditional recognition molecules [27]. Such advantages are: nontoxicity, dispersibility, ease of synthesis and modification, and good stability. Development of aptamer-based new techniques for tracking breast cancer subtypes is therefore of great significance.

Based on the above consideration, we herein constructed the new probe for differentiating breast cancer by combining target recognition property of the aptamer and fluorescence property of Ag NCs. As a proof of concept, the MUC1 aptamer that can specifically bind to the MUC1 mucin was used. The MUC1 mucin is a tumor marker in epithelial malignancies often used in immunotherapeutic and diagnostic approaches [28]. According to this design, the DNA template which is used to form the Ag NCs should contain three parts: Part one is a cytosine rich sequence that can be used to generate fluorescence Ag NCs; Part two is the linker which is generally composed of poly A or T; and Part three is the target recognizing sequence in the probe (Figure 1). Considering the DNA sequence dependence of the Ag NCs, the change in fluorescence properties for the Ag NCs, after functionalization with aptamer, is unpredictable. Meanwhile, the bright fluorescence from the aptamer-functionalized Ag NCs is essential for obtaining high resolution fluorescence images of cancer cells. It is therefore necessary to evaluate the effects of Part two and Part three on fluorescence properties of the aptamer-functionalized Ag NCs. In this study, the MUC1 aptamer was connected with C4A4C3 strand to form red fluorescence Ag NCs via poly A or T loop. The results demonstrated that the obtained Ag NCs could emit the red fluorescence (E_x/E_m was 560/605 nm) with high QY (66.5%) when –AAAAA– was used as linker which was further used to stain the MCF-7 breast cancer cells and differentiate them from MDA-MB-231 breast cancer cells and A549 human lung cancer cells.

2 Experimental

2.1 Materials

Sodium borohydride and silver nitrate (99.99%) were purchased from Sigma (USA). All the oligonucleotides were synthesized by Shanghai Sangon Biotechnology (China) Company and details are given in Table 1. Citric acid, sodium citrate, NaCl, NaOH, Na_2HPO_4, and NaH_2PO_4 were obtained from Shanghai Chemical Reagent Corporation (China). Mili-Q water (18.2 MΩ cm^{-1}) was used in all experiments.

2.2 Methods

2.2.1 Synthesis of silver clusters

All silver nanoclusters in this work were synthesized as prior reports with slight modification [16]. Briefly, 10 μL of DNA (100 μM) was mixed with 25 μL of phosphate buffer (80 mM, pH 6.6). $AgNO_3$ was then added into the above mixture solution according to DNA/Ag^+ (1:18) molar ratio. The mixture was reduced by adding 22.5 μL (400 μM) of freshly prepared $NaBH_4$ solution after 30 min of incubation at room temperature, followed by vigorous shaking for 10 s and storage in the dark before further experiment. The total reaction volume

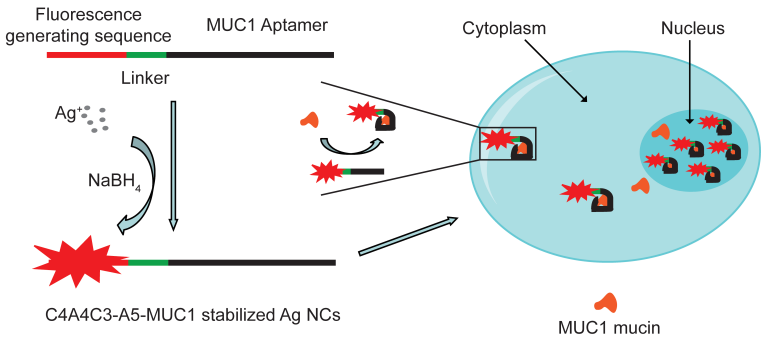

Figure 1 Schematic representation of MCF-7 breast cancer cells detection based on MUC1 apatmer functionalized Ag NCs. C4A4C3 sequence is connected with MUC1 aptamer via –AAAAA– linker. Silver ion is binding to C4A4C3 sequence and reduced to silver cluster. The synthesized Ag NCs get into cells and bind to MUC1 mucin after incubation with cells. MCF-7 breast cancer cells can be stained due to overexpression of MUC1 mucin. Partial enlarged details are schematic representation of combination between Ag NCs and MUC1 mucin (color online).

Table 1 Oligonucleotides used in this study

Name	Sequence (5′-3′)
C4A4C3	CCCCAAAACCC
C4A4C3-A4-MUC1	CCCCAAAACCCAAAAGCAGTTGATCCTTTGGATACCCTGG
C4A4C3-A5-MUC1	CCCCAAAACCCAAAAAGCAGTTGATCCTTTGGATACCCTGG
C4A4C3-A6-MUC1	CCCCAAAACCCAAAAAAGCAGTTGATCCTTTGGATACCCTGG
C4A4C3-T5-MUC1	CCCCAAAACCCTTTTTGCAGTTGATCCTTTGGATACCCTGG
C4A4C3-T8-MUC1	CCCCAAAACCCTTTTTTTTGCAGTTGATCCTTTGGATACCCTGG
C4A4C3-T10-MUC1	CCCCAAAACCCTTTTTTTTTTGCAGTTGATCCTTTGGATACCCTGG
MUC1-A5-C4A4C3	GCAGTTGATCCTTTGGATACCCTGGAAAAACCCCAAAACCC

was 100 μL.

2.2.2 Characterization of Ag NCs

Fluorescence of the Ag NCs was measured using F-7000 fluorescence spectrophotometer (Hitachi, Japan) at 25 °C. The emission/excitation spectra were obtained at an interval of 5 nm excitation wavelength. The UV-visible (UV-Vis) absorption spectra were performed with UV-1800 spectrophotometer (Shimadzu, Japan). Transmission electron microscope (TEM) images were taken with JEM-2100 transmission electron microscope (JEOL, Japan). The prepared Ag NCs were dropped on carbon-coated copper grids and dried at 25 °C. The average size of the Ag NCs was estimated using Nano Measurer software.

2.2.3 Cell culture

MCF-7 is one of the human breast cancer cell line whose MUC1 protein expression level is high while A549 is human lung cancer cell line whose MUC1 protein expression level is low and MDA-MB-231 is human breast cancer cells whose MUC1 protein expression level is low. All the three cell lines were obtained from Cell Resource Center of Shanghai Institute for Biological Sciences (Chinese Academy of Sciences, Shanghai, China). The MCF-7 cells were seeded in RPMI-1640 medium supplemented with 10% fetal bovine serum (FBS) and 100 IU mL^{-1} penicillin-streptomycin and incubated at 37 °C with 5% CO_2. The cell density was determined using hemocytometer. The other two types of cells were both cultured in Dulbecco's modified Eagle's medium (DMEM) and supplemented with 10% FBS and 100 IU mL^{-1} penicillin-streptomycin at 37 °C in humid atmosphere with 5% CO_2.

2.2.4 Confocal laser microscopy assay

Cells were seeded in a Lab-Tek 8-well chambered cover glass. The cells were then incubated with Ag NCs (30 μL of the above Ag NCs were formed with C4A4C3-A5-MUC1 under pH 6.6) after 24 h at 37 °C for 30 min. To remove the unbound Ag NCs, the cells were washed three times with phosphate buffer saline (PBS buffer, pH 7.4). The cells were finally observed under the confocal laser-scanning microscope (CLSM, Leica TCS-SP8, Germany) at 552 nm excitation wavelength.

3 Results and discussion

3.1 Effect of linker on fluorescence properties of MUC1 aptamer functionalized Ag NCs

To synthesize the new probe in one-pot, the DNA template used as the ligand should consist of both MUC1 aptamer and C4A4C3, which are further connected by the poly A or poly T linker as illustrated in Figure 1. It was hypothesized that the flexible spacer here could prevent the interference from these two regions. Considering the fluorescence dependence on sequence, the type and length of the linker were separately changed to study their effect on the fluorescence of Ag NCs. As shown in Figure 2(a), the linker strongly affected the fluorescence intensity, where the Ag NCs formed with the –AAAAA– linker showed bright red fluorescence, while the Ag NCs formed with the –TTTTT– linker showed very weak red fluorescence. The reason for these different results may stem from the nucleation of Ag^+ on the –AAAAA– loop or –TTTTT– loop, which could interfere with the synthesis of C4A4C3-linker-aptamer templated Ag NCs. It should be noted that the fluorescence intensity of Ag NCs with the –AAAAA– linker was higher than that of the C4A4C3 stabilized Ag NCs. We found that the position of the MUC1 aptamer also affected the fluorescence intensity of the Ag NCs. When the MUC1 aptamer was connected to the 3′ end of the C4A4C3, the fluorescence intensity of the resulting Ag NCs was about 4-fold more than that from the MUC1 aptamer connected to the 5′ end of the C4A4C3 (Figure 2(a)). Additionally, the effect of the linker length on the fluorescence intensity of the Ag NCs was also investigated. When the linkers with other lengths were used instead, the fluorescence intensities from the synthesized Ag NCs dropped to one sixteenth of the Ag NCs synthesized using the –AAAAA– linker (Figure 2(b)). The above phenomena may be ascribed to the steric hindrance between the aptamer and synthesized Ag NCs. Based on the above results, we concluded that the length and type of the linker strongly affected the fluorescence intensity and slightly influenced the emission wavelength of the MUC1 aptamer functionalized Ag NCs. In order

to obtain superior fluorescence probe, the –AAAAA– linker was selected for use in the following experiments.

3.2 Effect of synthesis conditions on fluorescence properties of C4A4C3-A5-MUC1 stabilized Ag NCs

High QY of the Ag NCs is beneficial for obtaining high-resolution cell images and achieving an optimal analytical performance. To obtain the Ag NCs with high QY, the experimental conditions for the synthesis of Ag NCs were further optimized through testing of pH and DNA/Ag^+ molar ratio. As illustrated in Figure 3(a), the fluorescence intensity of the Ag NCs stabilized by the C4A4C3-A5-MUC1 decreased with increased pH. The Ag NCs synthesized under acidic condition were much brighter (over 6 folds) than those obtained under the alkaline condition. As known, the fluorescence intensity of the DNA stabilized Ag NCs [29] is closely related to the secondary structure of DNA. At low pH, cytosine (pK_a 4.5) [30] is hemi-protonated and forms stable C–H^+–C mismatch or more stable C–Ag^+–C structure which influences the secondary structure of oligonucleotides. To meet the requirement for subsequent cell staining, pH 6.6 was selected to obtain the best staining results and simultaneously reduce the risk for cell death. It is worth mentioning that the optimum pH was 7.6 when using the C4A4C3 oligonucleotide as the template alone (Figure 3(b)), which was different from the aptamer functionalized Ag NCs, indicating that the effect of the pH on the fluorescence of Ag NCs was related to DNA length.

The effect of DNA/Ag^+ molar ratio (from 1:6 to 1:24) on the fluorescence intensity of Ag NCs was further studied in this work. As illustrated in Figure 3(c), the fluorescence intensity of the resulting Ag NCs first increased with increased amount of Ag^+, and reached maximum when the DNA/Ag^+ ratio was 1:18. The fluorescence intensity of the Ag NCs then decreased with further increase in the amount of Ag^+. As a

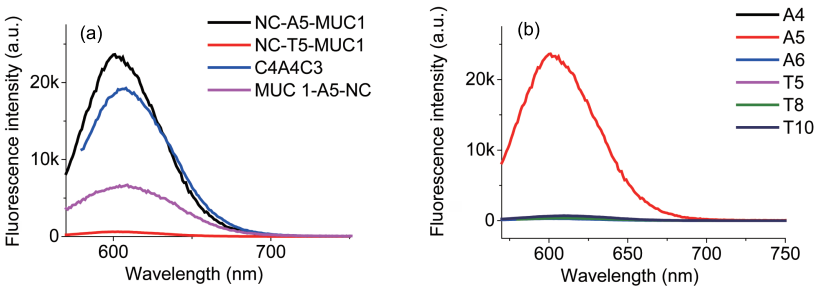

Figure 2 (a) Fluorescence emission spectra of Ag NCs combined with MUC1 aptamer at 5′ or 3′ end; (b) effect of linker length on the fluorescence emission of MUC1 aptamer functionalized Ag NCs. The excitation wavelength is 560 nm (color online).

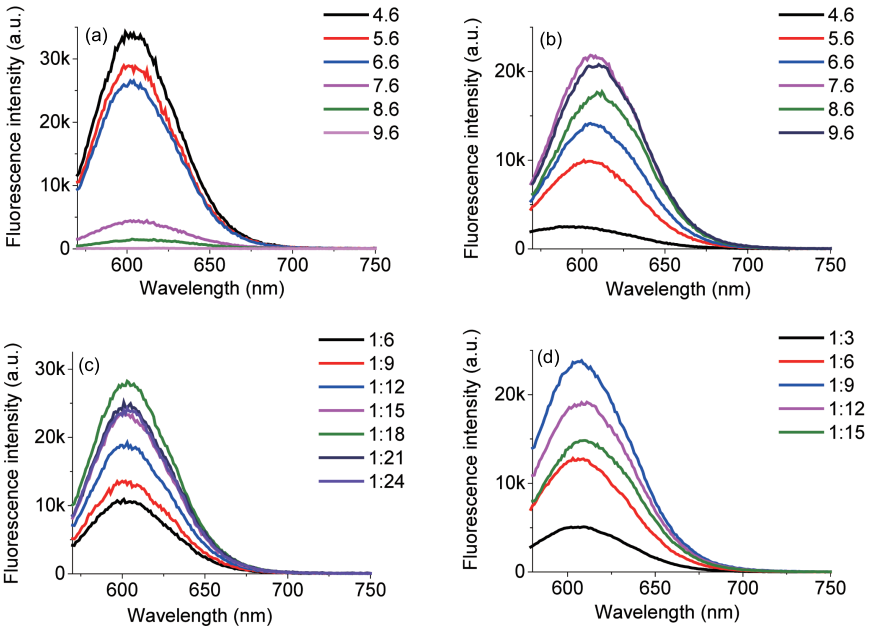

Figure 3 (a) Effect of pH on the fluorescence emission of C4A4C3-A5-MUC1 templated Ag NCs; (b) effect of pH on the fluorescence emission of C4A4C3 oligonucleotide templated Ag NCs; (c) effect of oligonucleotide/Ag^+ molar ratio on the fluorescence emission of C4A4C3-A5-MUC1 templated Ag NCs; (d) effect of oligonucleotide/Ag^+ molar ratio on the fluorescence emission of C4A4C3 oligonucleotide templated Ag NCs (color online).

control when using the C4A4C3 oligonucleotide as the template, the optimum molar ratio of DNA/Ag^+ was 1:9 (Figure 3(d)). The increase in Ag^+ dosage may be attributed to the increase in DNA length and longer DNA would attract more Ag^+ during the synthesis of Ag NCs.

We found that the parameters listed above also affected the reaction rate. Under the optimum conditions (pH 6.6 and DNA/Ag^+ molar ratio of 1:18 for C4A4C3-A5-MUC1 templated Ag NCs and 1:9 for C4A4C3-templated Ag NCs), the fluorescence intensity of Ag NCs, templated by C4A4C3-A5-MUC1, could reach maximum in 30 min, while it took about 20 h for the C4A4C3-templated Ag NCs to produce maximum fluorescence intensity (Figure 4).

3.3 Characterization of C4A4C3-A5-MUC1 templated Ag NCs

To better understand the optical properties of the C4A4C3-A5-MUC1 stabilized Ag NCs, we measured their UV-Vis spectra and fluorescence spectra. Two absorption peaks at 440 (weak) and 555 (strong) nm in the UV-Vis spectra corresponded to Ag nanoparticles and Ag nanoclusters, respectively (Figure 5(a)). The Ag NCs emitted fluorescence at 605 nm when excited at 560 nm, which was close to the designed excitation wavelength (552 nm) of the confocal laser microscopy. The emission spectra showed similar peaks when excited from 520 to 570 nm (Figure 5(b)), suggesting that there was only one type of fluorescence response from the Ag NCs. The QY of Ag NCs stabilized by C4A4C3-A5-MUC1 was also calculated. The QY of the Ag NCs stabilized with NC-A5-MUC1 was 66.5%, with rhodamine B (31%) in water as the reference standard. For the UV-Vis absorption spectrum from the C4A4C3-templated Ag NCs, three peaks at 365, 480 and 545 nm were observed (Figure 5(c)). As shown in Figure 5(d), there were two peaks of fluorescence emission at 550 and 610 nm when excited from 480 to 550 nm, respectively, indicating the formation of two types of fluorescent Ag NCs.

TEM images indicated that the Ag NCs templated by C4A4C3-A5-MUC1 were monodispersed with 2.0±0.4 nm in average diameter of (Figure 6(a, b)). Compared with the aptamer functionalized Ag NCs, the C4A4C3-templated Ag NCs were smaller (1.2±0.2 nm, Figure 6(c, d)). The increase in the size of the Ag NCs can be ascribed to longer length of the C4A4C3-A5-MUC1 strand as described earlier.

3.4 Cell staining by C4A4C3-A5-MUC1 stabilized Ag NCs

In order to prove our assumption that the resulting Ag NCs

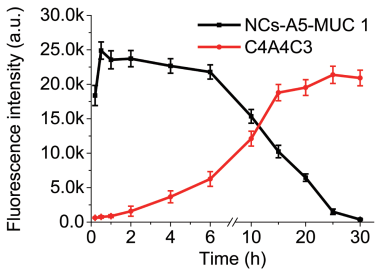

Figure 4 Temporal change in fluorescence intensity of C4A4C3-A5-MUC1 and C4A4C3 templated Ag NCs. The excitation and emission wavelengths are 550 and 610 nm, respectively (color online).

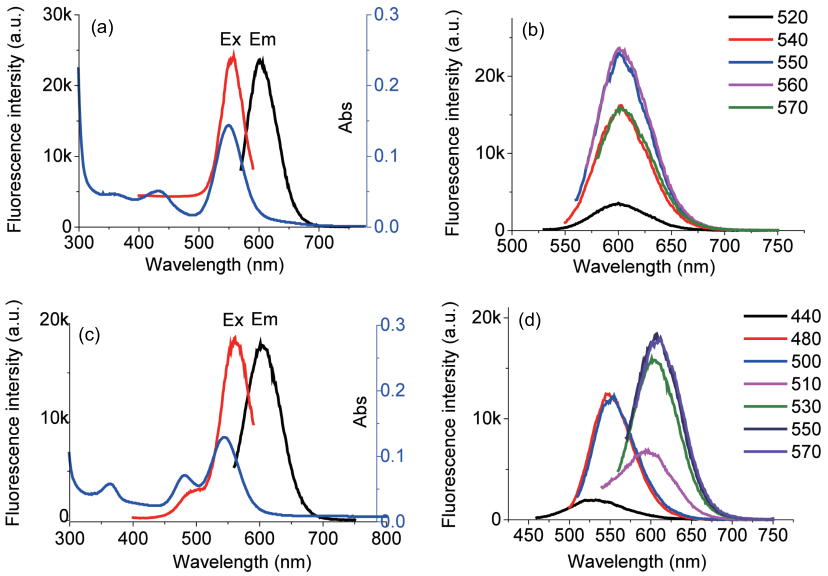

Figure 5 (a) Ultraviolet absorption spectra and fluorescence emission spectra of C4A4C3-A5-MUC1 templated Ag NCs; (b) fluorescence emission spectra of C4A4C3-A5-MUC1 templated Ag NCs excited at various wavelengths; (c) ultraviolet absorption spectra and fluorescence emission spectra of C4A4C3 oligonucleotide templated Ag NCs; (d) fluorescence emission spectra of C4A4C3 oligonucleotide templated Ag NCs excited at various wavelength (color online).

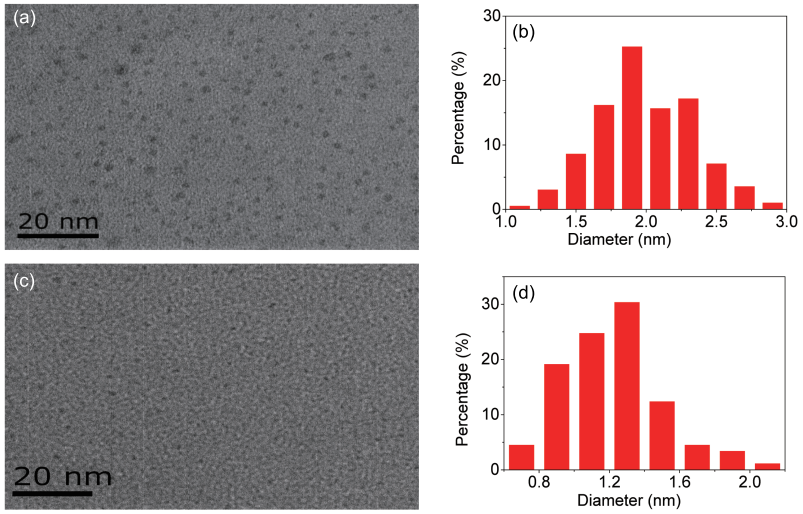

Figure 6 (a) TEM image of C4A4C3-A5-MUC1 templated Ag NCs; (b) particle size distribution of Ag NCs (the mean diameter is 2.0±0.4 nm); (c) the TEM image of C4A4C3 oligonucleotide templated Ag NCs; (d) particle size distribution of Ag NCs (the mean diameter is 1.2±0.2 nm) (color online).

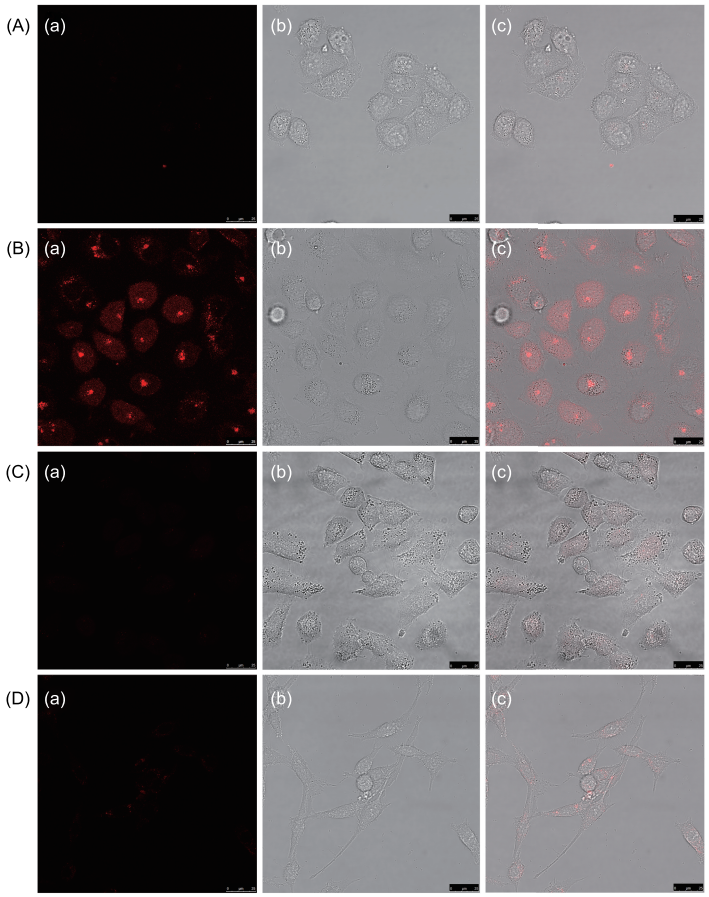

Figure 7 Confocal laser scanning microscopy of (A) MCF-7 human breast cancer cells without staining, (B) MCF-7 human breast cancer cells, (C) MDA-MB-231 human breast cancer cells, (D) A549 human lung cancer cells incubated with C4A4C3-A5-MUC1 stabilized Ag NCs at 37 °C for 30 min. (a) Ag NCs fluorescence images; (b) bright-field images; (c) overlapping of corresponding fluorescence image and bright-field image. The Ag NCs were excited with 552 nm (color online).

could be used as the fluorescent probe in breast cancer cell staining and imaging, we tested the binding affinity of the Ag NCs by incubating them with MCF-7 cells, A549 cells, and MDA-MB-231 cells separately. All the cell lines showed varied MUC1 expression. After incubation at 37 °C for 30 min, these cells were observed using confocal laser scanning

microscopy. As shown in Figure 7(A), the MCF-7 cells showed no signal when excited at 552 nm, indicating that there was no autofluorescence from the cells. However, after incubation with Ag NCs, the MCF-7 cells showed red fluorescence (Figure 7(B)), suggesting excellent binding affinity between the C4A4C3-A5-MUC1 probe and MUC1 protein. Moreover, to detect different breast cancer cells based on their differential expression of MUC1 protein, the MDA-MB-231 cells were selected as contrast breast cancer cells. As illustrated in Figure 7(C), the MDA-MB-231 cells could not be stained with C4A4C3-A5-MUC1 stabilized Ag NCs due to low expression level for the MUC1 protein. The A549 cells are human lung cancer cells and do not express the MUC1 protein. Therefore, these cells could not be recognized by the AgNCs (Figure 7(D)). These results indicated that the C4A4C3-A5-MUC1 stabilized Ag NCs could specifically bind with MUC1 protein and recognize the MCF-7 cells because of their high expression level for the MUC1 protein. The other cell lines expressing low-level MUC1 protein could not be detected.

4 Conclusions

In this study, Ag NCs with bright red emission were successfully synthesized by using C4A4C3-A5-MUC1 as the template through one-pot process. The fluorescence quantum yield of the Ag NCs reached up to 66.5% with rhodamine B as the reference standard. A series of preliminary experiments were firstly conducted during the research to optimize various reaction parameters, including length and type of linker, pH, and DNA/Ag^+ molar ratio. In comparison with the C4A4C3-templated Ag NCs, lower pH and more Ag^+ dosage were required for the synthesis of C4A4C3-A5-MUC1 stabilized Ag NCs. The cell staining results indicated that only MCF-7 breast cancer cells, among the three studied cell lines, could be recognized by the C4A4C3-A5-MUC1 stabilized Ag NCs, depending on the binding affinity of the MUC1 aptamer to MUC1 protein. Compared with other techniques used in the breast cancer subtyping, this strategy of using the aptamer functionalized Ag NCs is cheap and simple. It is expected that more corresponding aptamer functionalized Ag NCs will be developed and used for breast cancer cell-typing, with more aptamers to be found in the future, which could also recognize different breast cancer cell types.

Acknowledgments This work was supported by the National Basic Research Program of China (2014CB744501), the National Natural Science Foundation of China (61271056, 61527806), the Natural Science Foundation of Jiangsu Province (BK20141332), the National Youth Science Foundation of China (61301043), the Priority Academic Program Development of Jiangsu Higher Education Institutions, and the Fundamental Research Funds for the Central Universities.

Conflict of interest The authors declare that they have no conflict of interest.

1 Yeh HC, Sharma J, Han JJ, Martinez JS, Werner JH. *Nano Lett*, 2010, 10: 3106–3110
2 Yang SW, Vosch T. *Anal Chem*, 2011, 83: 6935–6939
3 Sharma J, Yeh HC, Yoo H, Werner JH, Martinez JS. *Chem Commun*, 2011, 47: 2294–2296
4 Lee J, Park J, Lee HH, Kim HI, Kim WJ. *J Mater Chem B*, 2014, 2: 2616–2621
5 Yin J, He X, Wang K, Qing Z, Wu X, Shi H, Yang X. *Nanoscale*, 2012, 4: 110–112
6 Li J, Zhong X, Cheng F, Zhang JR, Jiang LP, Zhu JJ. *Anal Chem*, 2012, 84: 4140–4146
7 Yin J, He X, Wang K, Xu F, Shangguan J, He D, Shi H. *Anal Chem*, 2013, 85: 12011–12019
8 Ono A, Cao S, Togashi H, Tashiro M, Fujimoto T, Machinami T, Oda S, Miyake Y, Okamoto I, Tanaka Y. *Chem Commun*, 2008, 39: 4825
9 Okamoto I, Iwamoto K, Watanabe Y, Miyake Y, Ono A. *Angew Chem Int Ed*, 2009, 48: 1648–1651
10 Megger DA, Fonseca Guerra C, Hoffmann J, Brutschy B, Bickelhaupt FM, Müller J. *Chem Eur J*, 2011, 17: 6533–6544
11 Ono A, Torigoe H, Tanaka Y, Okamoto I. *Chem Soc Rev*, 2011, 40: 5855–5866
12 Yang X, Gan L, Han L, Wang E, Wang J. *Angew Chem Int Ed*, 2013, 52: 2022–2026
13 Zhou XH, Kong DM, Shen HX. *Anal Chem*, 2010, 82: 789–793
14 Gwinn EG, O'Neill P, Guerrero AJ, Bouwmeester D, Fygenson DK. *Adv Mater*, 2008, 20: 279–283
15 Richards CI, Choi S, Hsiang JC, Antoku Y, Vosch T, Bongiorno A, Tzeng YL, Dickson RM. *J Am Chem Soc*, 2008, 130: 5038–5039
16 Li T, He N, Wang J, Li S, Deng Y, Wang Z. *RSC Adv*, 2016, 6: 22839–22844
17 Xi Z, Huang R, Li Z, He N, Wang T, Su E, Deng Y. *ACS Appl Mater Interfaces*, 2015, 7: 11215–11223
18 Zhao X, Huang Y, Yang CJ, Mao B. *Sci China Chem*, 2015, 58: 1858–1865
19 Xi Z, Huang R, Deng Y, He N. *J Biomed Nanotechnol*, 2014, 10: 3043–3062
20 Guo F, Hu Y, Yu L, Deng X, Meng J, Wang C, Yang XD. *J Nanosci Nanotechnol*, 2016, 16: 2246–2253
21 Sun Z, Wang Y, Wei Y, Liu R, Zhu H, Cui Y, Zhao Y, Gao X. *Chem Commun*, 2011, 47: 11960–11962
22 Jiang H, Xu G, Sun Y, Zheng W, Zhu X, Wang B, Zhang X, Wang G. *Chem Commun*, 2015, 51: 11810–11813
23 Ludwig JA, Weinstein JN. *Nat Rev Cancer*, 2005, 5: 845–856
24 Won JY, Choi JW, Min J. *Biosens Bioelectron*, 2013, 40: 161–166
25 Jayasena SD. *Clinic Chem*, 1999, 45: 1628–1650
26 Huang R, Xi Z, He N. *Sci China Chem*, 2015, 58: 1122–1130
27 Kong RM, Chen Z, Ye M, Zhang XB, Tan WH. *Sci China Chem*, 2011, 54: 1218–1226
28 Ferreira CSM, Papamichael K, Guilbault G, Schwarzacher T, Gariepy J, Missailidis S. *Anal Bioanal Chem*, 2008, 390: 1039–1050
29 Li J, Jia X, Li D, Ren J, Han Y, Xia Y, Wang E. *Nanoscale*, 2013, 5: 6131–6138
30 Sengupta B, Springer K, Buckman JG, Story SP, Abe OH, Hasan ZW, Prudowsky ZD, Rudisill SE, Degtyareva NN, Petty JT. *J Phys Chem C*, 2009, 113: 19518–19524